# CO-POLAR CORRELATION MEASUREMENTS OF PRECIPITATION

Anthony J. Illingworth and I. Jeff Caylor

Dept of Pure and Applied Physics
UMIST, Manchester, M60 1QD, UK

## 1. INTRODUCTION

The co-polar correlation is primarily a measure of the variety of shapes and fall modes of precipitation particles and provides information on the types of hydrometeors present within clouds. The observations are made at S-band using the RAL Chilbolton dual polarisation radar situated in Hampshire, England. This radar (Goddard and Cherry, 1987) can transmit (and receive) pulses every 1.6msec which are alternately polarized in the horizontal and vertical directions. The pulses are 0.5usec long with a peak power of 500kW. The return power is digitised every 500nsec to give 75m range resolution.

Figure 1 shows time series data for 210msec obtained at a single 75m gate from 64 pulse pairs transmitted and received with alternate polarization providing 64 samples of $Z_H$ and $Z_V$, the reflectivities for horizontal and vertical polarization respectively.

The differential reflectivity, $Z_{DR}$, is defined:

$$Z_{DR} = 10\log(Z_H / Z_V) \qquad (1)$$

where $Z_H$ and $Z_V$ are the average (linear power) of the 64 samples, as shown by the straight lines in Figure 1. These data are for drizzle and, as the particles are all spherical, $Z_{DR}$ is zero and the correlation is very close to unity.

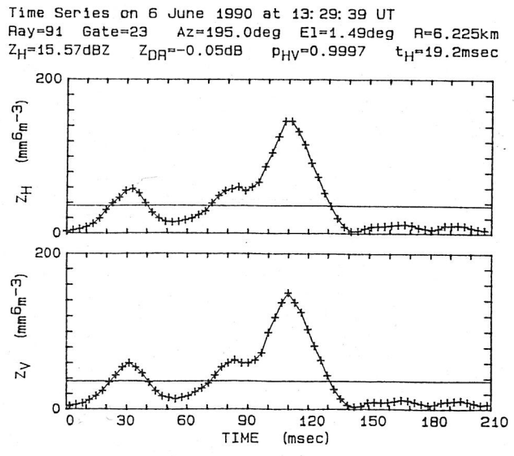


Fig 1. $Z_H$ and $Z_V$ time series in drizzle. $\rho$=0.997.

## 2. THEORETICAL VALUES OF $\rho_{HV}$

The complex correlation between the horizontally and vertically polarised returns is defined as:

$$\rho(0)_{HV} = \langle HV^* \rangle / (\langle H^2 \rangle \langle V^2 \rangle)^{0.5} \qquad (2)$$

where H and V are the amplitudes of the horizontally and vertically polarised returns, (0) indicates simultaneous sampling, and the angled brackets signify an ensemble average. Sachidananda and Zrnic (1985) show that:

$$|\rho(0)_{HV}| = \frac{\sum S_{11}S_{22}}{(\sum S_{11}^2 \sum S_{22}^2)^{0.5}} \qquad (3)$$

where $S_{11}$ and $S_{22}$ are proportional to the diagonal (co-polar) elements of the scattering matrix. At S-band we may assume Rayleigh scattering and so the elements are real. For brevity we shall use the term $\rho$ for $|\rho(0)_{HV}|$.

### 2.1 Theoretical $\rho_{HV}$ of rain.

The expected correlations in rain have been computed from Equation 3 assuming an exponential drop size distribution of the form

$$N(D) = N_o \exp(-3.67D / D_o) \qquad (4)$$

As $D_0$ (the volume median drop diameter) increases, $\rho$ falls and $Z_{DR}$ increases, but the actual values of $\rho$ for a given $Z_{DR}$ depend upon the assumed raindrop shapes and the maximum drop size, $D_m$, at which the spectrum is truncated. The solid line in Figure 2 is for the Beard and Chuang (1987)

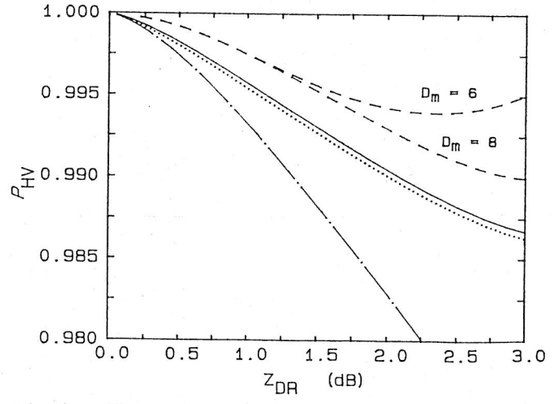


Fig 2. Theoretical values of $\rho$ in rain for an exponential drop size distribution.
Drop shapes: —— Beard and Chuang,
----- Green.
Oscillating drops: ..... Chandrasekar et al,
.-.-.-. Beard et al.

American Meteorological Society
25th Conference on Radar Meteorology
Paris, France
24-28 June 1991

drop shapes with a $D_m$ of 8mm; this model gives the best agreement with ZDR observations (Illingworth and Caylor, 1989). It is computationally convenient to use Green's (1975) approximate analytic expression for the drop shape as a function of D but the predicted correlations are higher by about 0.005. Truncation of the drop size distribution at 6mm (Sachidananda and Zrnic, 1987) would lead to a rise of $\rho$ for $Z_{DR}$ values of about 2dB.

### 2.2 Effects of Raindrop Oscillation

There has been much debate about the effects of raindrop oscillations on polarisation parameters. Based upon aircraft images of raindrops Chandrasekar et al (1988) suggest that the amplitude of oscillation of raindrops is equal to a change in axial ratio of 0.1; theory (using Beard and Chuang shapes) shows that this would lead to a quite negligible reduction of 0.0005 in values of $\rho$ (Figure 2). Beard et al (1989) have shown that the axial ratio of 1.4mm raindrops oscillates between 0.91 and 1.05. If their suggestion that larger drops oscillate with similar amplitude is correct, then $\rho$ is reduced drastically as shown in Figure 2, where we have assumed that the amplitude is such that the extreme shape is spherical. Because these oscillations are not seen in in-situ observations, we predict that their effect on $\rho$ will be insignificant and in all but the heaviest rain $\rho$ should be above 0.985.

### 2.3 Theoretical $\rho_{HV}$ of Ice and the Bright Band

Definitive theoretical computations of correlation for ice particles and the bright band are not possible because of the unknown variety of shapes, sizes, and fall modes of the frozen and melting particles. If we assume all particles have the same shape but are randomly tumbling, then application of Equation 3 predicts:

$$|\rho_{HV}| = \frac{6Z_{DRI} + 8\sqrt{Z_{DRI}} + 1}{8Z_{DRI} + 4\sqrt{Z_{DRI}} + 3} \qquad (5)$$

where we follow Jameson (1987) in defining the intrinsic $Z_{DR}$ ($Z_{DRI}$) as the $Z_{DR}$ the particles would have if they were aligned with their minor axes vertical. Values of $Z_{DRI}$ ($=(S_{11}/S_{22})^2$) as a function of axial ratio for wet particles and for different types of ice are shown in Figure 3 and values of $\rho$ from Equation 5 are plotted in Figure 4. These figures suggest that, because of its very low $Z_{DRI}$, snow should have a $\rho$ of 0.999 (higher than most rain), and that dry graupel with an axial ratio of 0.8 will have a similar value, falling to about 0.993 if wet. Very oblate (axial ratio 0.3, $Z_{DRI}$ 10dB) melting snow could have a $\rho$ of about 0.9. If the particles are not randomly tumbling, but are merely rocking and gyrating with a Gaussian distribution of canting angles about the horizontal axis, then the correlation will not be so low. Figure 4 also shows that lower values of $\rho$ are possible for a mixture of 50% tumbling and 50% aligned particles, this may be appropriate for melting snow, where values down to 0.81 appear possible. Mie scattering could give lower values of $\rho$ but is not relevant in the UK at S-band.

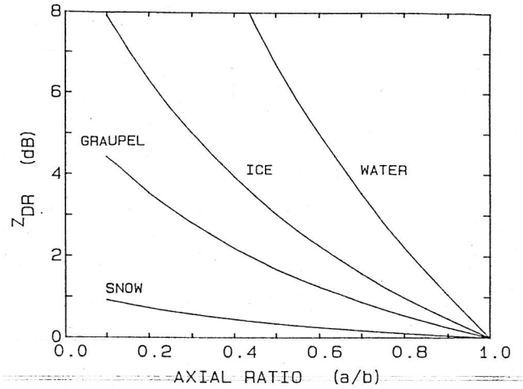


Fig 3. Values of $Z_{DR}$ of aligned particles ($Z_{DRI}$) for various axial ratios. Graupel has density 0.5 and snow has 0.1 g/m$^3$.

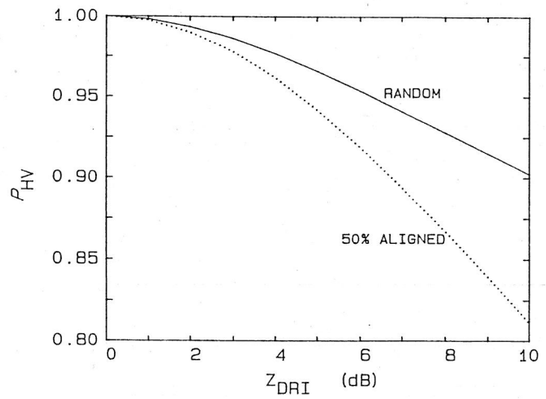


Fig 4. Theoretical $\rho$ for oblate spheroids all having the same $Z_{DRI}$. —— randomly tumbling, .... 50% aligned and 50% tumbling.

## 3. ESTIMATING $\rho_{HV}$ FROM THE TIME SERIES

To derive $\rho$ from the time series we make the fundamental assumption that the successive estimates of $\rho$ are equivalent to the different configurations in space of the ensemble. Rogers and Walker (1973) show that for a square law detector, and summing over successive samples:

$$|\rho_{HV}|^2 = \frac{\sum Z_H Z_V}{\left(\sum Z_H^2 \sum Z_V^2\right)^{0.5}} \qquad (6)$$

### 3.1 Signal to Noise Problems

In Figure 5 we show that the predicted reduction in $\rho$ to an effective value $\rho^*$ by a signal to noise ratio, SNR, (Bringi et al, 1983)

$$\rho_{HV}^* = \frac{\rho_{HV}}{(1 + 1/SNR)^{0.5}\,(1 + Z_{DR}/SNR)^{0.5}} \qquad (7)$$

is in good agreement with $\rho$ from dwells in very thick widespread drizzle. Different values of

SNR were obtained by using data at various ranges from the radar and an interpolation algorithm (see below) was used to compensate for the staggered sampling. Each data point is for a 1dB step in SNR and is the mean $\rho$ from about 300 time series. The highest values of $\rho$ are not unity but are 0.997 to 0.998, equivalent to a SNR of 26dB; we believe this is an instrumental effect and could arise from a slight asymmetry in the sidelobes of the Chilbolton antenna or a starting jitter of 1nsec in the magnetron.

### 3.2 The Effect of Staggered Sampling

The effect of non-simultaneous sampling on the calculated correlations is shown in Figure 6. These data are for rain with a $Z_{DR}$ below 0.5dB and a SNR above 30dB which should have a $\rho$ of 0.998 (Figure 2), but as the time series have progressively shorter decorrelation times ($\tau$) the uncorrected 'raw' value of $\rho$ is reduced. $\tau$ is defined as the time for the autocorrelation to fall to 1/e. The data are binned in 1msec steps in $\tau$ with about 300 samples per bin. The efficiencies of two correction algorithms are also displayed in Figure 6. If a Gaussian velocity spectrum is assumed, (Sachidananda and Zrnic, 1985) then:

$$|\rho(0)_{HV}| - |\rho(1)_{HV}| \;/\; |\rho(2)_{HH}|^{0.25} \qquad (8)$$

where $|\rho(1)_{HV}|$ is the 'raw' value of $\rho$ for one pulse delay and $|\rho(2)_{HH}|$ is the autocorrelation of the H time series after two pulse intervals. The second correction algorithm does not assume any velocity spectrum but involves expressing the two time series as frequency spectra using an FFT and then computing the interpolated simultaneous samples from the frequency components. For these data the FFT technique gives mean $\rho$ equal to 0.997, the value for rain from the theory in Figure 2, over the copmplete range of $\tau$. The FFT approach is preferred and is used for all subsequent data in this paper.

### 3.3 Accuracy of the $\rho_{HV}$ Estimates

We now consider how many time series are needed to obtain a reliable estimate of the correlation. Figure 7 shows the mean and the standard deviation of $\rho$ during a 15 second dwell in rain, the bright band and in dry ice. The mean values agree well with theoretical predictions. It is clear that the standard deviation ($\sigma$) becomes larger as $\rho$ falls; this and other data confirm the empirical relationship that $\sigma$ is proportional to (1 - p) and for n time series a good approximation to the standard error, SE, is:

$$SE = \sigma/\sqrt{n} = 1.25(1 - \rho_{HV})/\sqrt{n} \qquad (9)$$

Equation 9 can be applied to the observations in Figure 7; if n is 60, then SE is equal to $\sigma/\sqrt{60}$, and we may say that the value of $\rho$ in the bright band at 14km range is 0.85±0.02.

Figure 8 demonstrates again how the spread of $\rho$ values increases as $\rho$ falls from unity. 1500 values of $\rho$ (15 gates, 25 sec) are used in both the bright band and in drizzle and are sorted into bins of width 0.1 log(1 - p). For these long dwells the standard errors can become very small: the mean $\rho$ is 0.9974±0.00005 for drizzle and for the bright band $\rho$ is 0.8490±0.003.

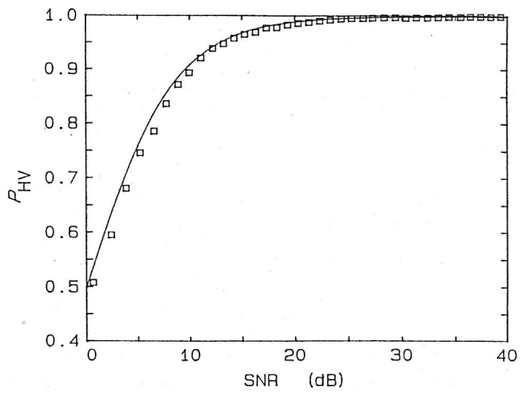


Fig 5. Effective $\rho$ in drizzle as a function of signal to noise ratio. Solid line from the theory of Bringi et al (1983).

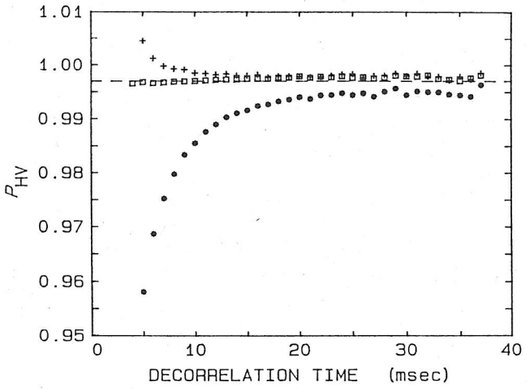


Fig 6. Comparison of techniques to correct for staggered sampling. ****** 'raw' uncorrected
□□□□□□ FFT technique
++++++ Gaussian spectrum.

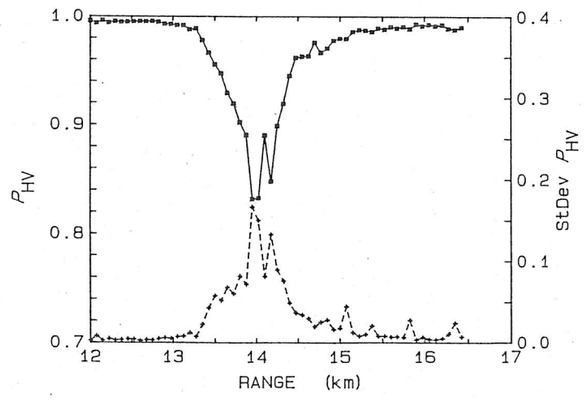


Fig 7. Mean values and standard deviation ($\sigma$) of $\rho$ for rain (12-13km), the bright band (14km) and dry ice (16km). Radar dwells for 60 time series (15 secs) at each 75m gate.

## 4. CORRELATION MEASUREMENTS IN RAIN

The correlation measures the variety of drop shapes present in rain and so should provide an estimate for the index, m, in a gamma function representation of the raindrop spectra:

$$N = N_o D^m \exp(-(3.67+m) / D_o) \qquad (10)$$

In Figure 9 rain data with various $Z_{DR}$ values are compared with the gamma function for various values of m using the Beard and Chuang drop shapes. Each data point is for 80 time series, with the standard error plotted as an error bar. Inspection shows that these errors are in agreement with Equation 9, for a mean ρ of 0.99 the SE is about 0.002. Such errors are typically the difference in ρ for a change of 2 in the index, m. It is difficult to make a definitive statement about the value of m from these observations but if the system has a SNR of 26dB then, from Equation 5, it is tempting to increase all values of ρ by a factor of 1.002 and the values of m are in the range 0 to 2.

## 5. MEASUREMENTS IN ICE AND THE BRIGHT BAND

Once the standard error (Eq. 9) is known, we can state the precision of the ρ estimate and explore the possibility of differentiating the various types of ice. These ρ agree with the predictions in Section 2.3. Low values of ρ of 0.9 and down to nearly 0.8 (see Figure 7) are found in the melting snow of the bright band. In dry snow ($Z_{DR}$ < 0.5dB) values are limited by system noise to about 0.997, slightly lower values can occur for higher $Z_{DR}$. ρ of 0.99 has been observed for melting graupel, but for dry graupel ρ is so near unity that any deviation is larger than the system noise.

## 6. APPLICATIONS AND CONCLUSIONS

The observed values of correlation in rain, ice and the bright band are in good agreement with theoretical predictions. For rain the Beard and Chuang shapes should be used but ρ values are inconsistent with the Green drop shapes and with truncating drop spectra at 6mm. Drop oscillations appear to have a negligible effect on ρ.

The lowest values of ρ are found in the bright band for melting snow. For other hydrometeors the changes are small, and may be masked if the signal to noise ratio of the radar system is poor. ρ values can easily be degraded by a poor interpolation algorithm of by the presence of small amounts of ground clutter. An empirical expression for the standard error of the ρ estimate is presented; these errors seem much lower than those predicted by Balakrishnan and Zrnic (1990). One application of ρ may be in recognising the bright band and correcting rainfall estimates derived from reflectivity measurements in operational radar networks.


## 7. ACKNOWLEDGEMENTS

The work was supported by NERC grants GR3/5896, AFOSR 88-0121, JCMM (Reading) and the Meteorological Office. We thank our co-workers J.W.F. Goddard and J. Eastment at the RAL Chilbolton radar.


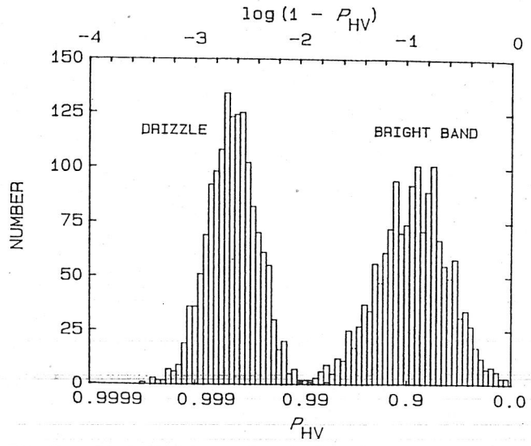


Fig 8. Distribution values of ρ from 1500 time series in rain and in the bright band. (15 adjacent gates, 25 second dwell).

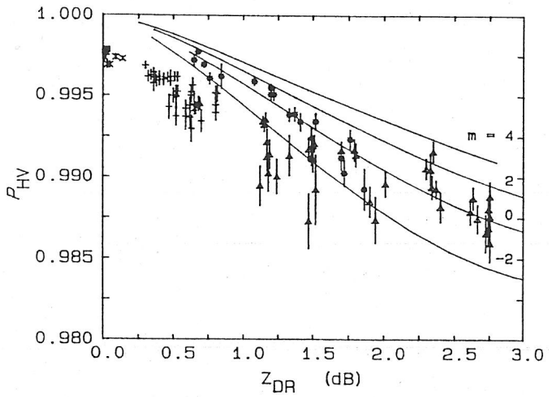


Fig 9. Mean values of ρ in rain. Vertical lines are the standard error for 80 time series. Solid lines are the theoretical values for various values of m in the gamma function.

## 8. REFERENCES


Balakrishnan N. and Zrnic D.S. (1990) J Atmos Sci, 47, 1525-1540.

Beard K.V. and Chuang C. (1987) J Atmos Sci, 44, 1509-1524.

Beard K.V., Ochs H.T. and Kubesh R.J. (1989) Nature, 342, 408-410.

Bringi V.N., Seliga T.A. and Cherry S.M. (1983) IEEE Trans Geo and Rem Sens, GE-21, 215-220.

Chandresakar V., Cooper W.A. and Bringi V.N. (1988) J Atmos Sci, 45,1323-1333.

Goddard J.W.F. and Cherry S.M. (1987) ICAP-87, IEE Conf Publ. 274, London, 325-327.

Green A.W. (1975) J Appl Met, 14, 1578-1583.

Illingworth A.J. and Caylor I.J. (1989) J Atmos Ocean Tech, 6, 939-949.

Jameson A.R. (1987) J Tech, 4, 634-645.

Rogers R.R. and Walker G.B. (1973) J Appl Met, 12, 1078-1080.

Sachidananda M. and Zrnic D.S. (1985) Rad Sci, 20, 907-922.

Sachidananda M. and Zrnic D.S. (1987) J Atmos Ocean Tech, 4, 588-598.